Comparison of the Notched Fatigue Life of Ti-10V-2Fe-3A1 and Ti-6A1-4V

G. R. Yoder*
Office of Naval Research, Arlington, Virginia
S. J. Gill*
Naval Research Laboratory, Washington, D.C.
and
R. R. Boyer†
Boeing Commercial Airplane Company, Seattle, Washington

The present study was undertaken in an effort to better understand the notched fatigue life behavior of Ti-10V-2Fe-3A1 alloy and its origins. In this work, the effects of metallurgical variables (viz., alpha phase aspect ratio and strength level) have been determined on the resistance to both fatigue crack initiation and propagation. From these data, computations were made to synthesize notched fatigue life for the different microstructural conditions. For this purpose, crack propagation life was integrated for the same specimen geometry and loading conditions for which a notched fatigue life question was raised in prior work. Similar computations were made for a variety of Ti-6A1-4V microstructural conditions for which counterpart data were available. Of prime significance, the results indicate that notched fatigue life of Ti-10V-2Fe-3A1 at the 190 ksi (1310 MPa) strength level is substantially superior to that of Ti-6A1-4V for the respective conditions examined. Moreover, it was found that a reduction in strength level of Ti-10V-2Fe-3A1 to 150 ksi (1034 MPa) ultimate tensile strength can degrade notched fatigue life to levels associated with the Ti-6A1-4V microstructures.

Introduction

THE advanced, near-beta Ti-10V-2Fe-3A1 alloy was successfully developed as a high-strength and toughness alloy with excellent forgeability.[1-3] Though a wide spectrum of attractive strength-level and fracture-toughness combinations has been demonstrated, there is substantial interest in this alloy for use at strength levels of 180 ksi (1241 MPa) and beyond, where potential weight savings are greatest. Unfortunately, preliminary data at the 180 ksi (1241 MPa) strength level indicated that although notched fatigue life was significantly superior to Ti-6A1-4V in the high-cycle regime, it appeared inferior in the low-cycle regime.[1,4] Consequently, the issue of notched fatigue life of this alloy in the high-strength condition has served as a barrier to its implementation in fatigue-critical applications. Indeed, the results of additional work have suggested that it may be necessary to reduce the strength level to the 150 ksi (1034 MPa) level to obviate the problem.[4,5] To date, however, the origins of the problem have remained elusive.

Thus, the present study was undertaken in an effort to better understand the notched fatigue resistance of Ti-10V-2Fe-3A1 and its origins. In this work, the effects of metallurgical variables have been separately determined on the resistance to fatigue-crack initiation and fatigue-crack propagation, using previously established techniques.[6,7] For this purpose, pancake forgings were examined as a function of processing and strength-level extremes. From the respective fatigue-crack initiation and fatigue-crack propagation data, computations were made to synthesize notched fatigue life for the different microstructural conditions. For this purpose, crack-propagation life was integrated, assuming Dowling's criterion for the point of demarcation between initiation and propagation phases of fatigue cracking in a notched region.[8] This was done for the specimen geometry (center-hole tension) for which the alleged notched fatigue-life problem was originally reported. Then, for comparative purposes, similar computations were made for a variety of Ti-6A1-4V microstructural conditions for which resistance to both fatigue-crack initiation and fatigue-crack propagation was previously established.[9,10]

Experimental Procedure

The detailed chemistry of the Ti-10V-2Fe-3A1 alloy is shown in Table 1. Four pancake forgings of this alloy were processed above the beta transus. One pair was then given 2% final work in the two-phase alpha/beta region, and the other pair 55%. One forging from each pair was solution heat treated and aged to produce an ultimate tensile strength (UTS) of approximately 190 ksi (1310 MPa); the others were heat treated to a nominal UTS level of 150 ksi (1034 MPa). Details of the respective solution treatment and aging schedules are shown in Table 2. The resulting mechanical properties are given in Table 3 along with estimates of toughness (K_{Ic}) from Ref. 4 and the present work. Microstructures associated with these four pancake forgings are displayed in Fig. 1, which indicates that the aspect ratio of the primary alpha phase varies inversely with percent final alpha/beta work, as intended. The data shown in Table 3 indicate that uniaxial tensile ductility decreases with increasing aspect ratio for each nominal strength level, though the plane strain fracture toughness increases. These trends are consistent with the observations of Hirth and Froes.[11] For dimensions of the pancake forgings and further information regarding processing, the reader is urged to consult Ref. 4.

To measure the resistance of each Ti-10V-2Fe-3A1 pancake forging to fatigue-crack initiation in the presence of a notch, a pair of compact-type (CT) specimens[12] were machined from the limited material available to the following nominal dimensions: a thickness B of 0.22 in. (5.6 mm), a width W of 2.0 in. (50.8 mm), an initial "crack" (notch) length a of 0.40 in. (10.2

Presented as Paper 87-0756 at the AIAA/ASME/ASCE/AHS 28th Structures, Structural Dynamics, and Materials Conference, Monterey, CA, April 6-8, 1987; received Jan. 1, 1988; revision received July 13, 1988.

*Metallurgist.
†Research Engineer.

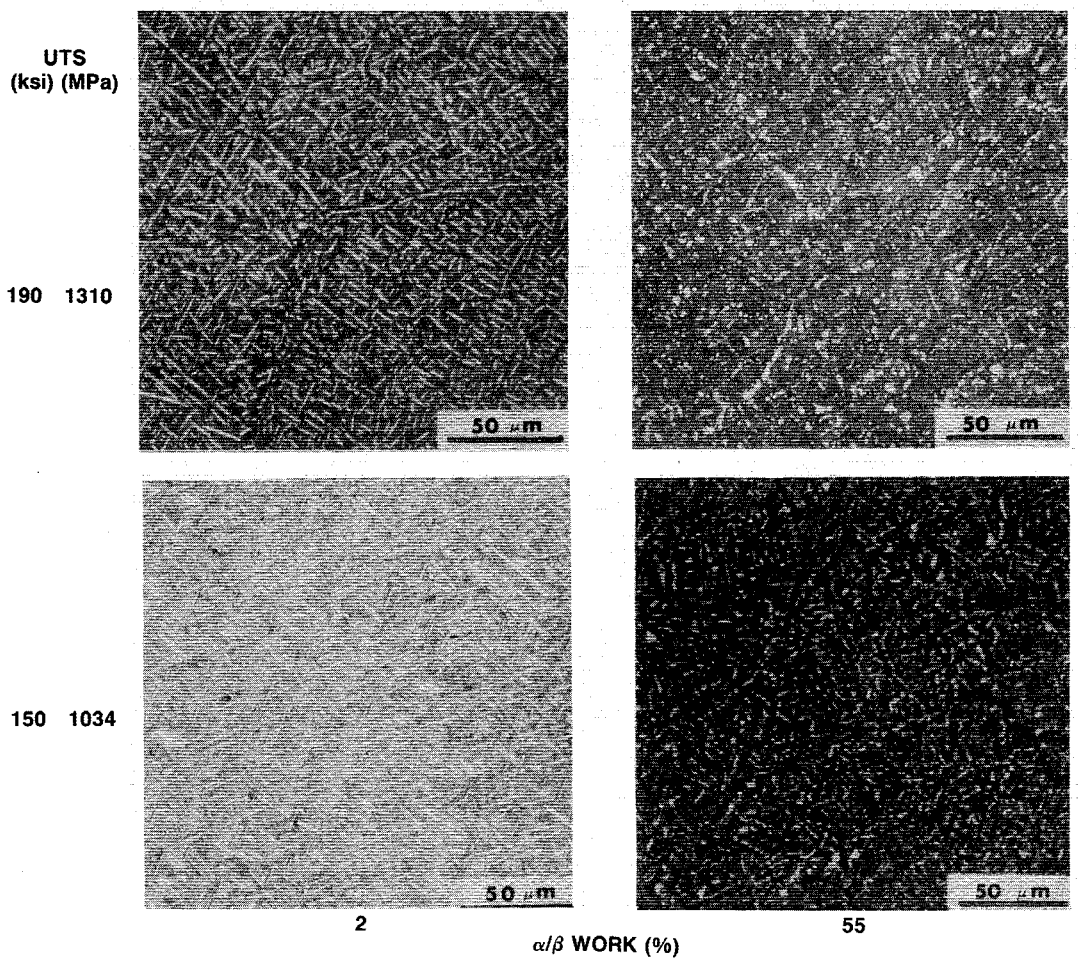

Fig. 1 Microstructures of Ti-10V-2Fe-3Al as function of strength level (UTS) and percent final α/β work.

mm), and a carefully honed notch root radius ρ of 0.010 in. (0.254 mm). Notch root surfaces were examined at 10–50X magnification in a stereo-zoom microscope to verify the complete removal of any tool marks parallel to the axis of the notch root (i.e., in the thickness direction). This procedure is important to ensure the subsequent measurement of inherent material resistance to fatigue-crack initiation.[7]

All specimens were cyclically loaded with a stress ratio of $R = 0.10$ and a haversine waveform. Notch root surfaces were systematically inspected for earliest indications of crack initiation, using a low-powered traveling microscope. Notched fatigue-crack initiation resistance is commonly reported in terms of the parameters $\Delta K/\sqrt{\rho}$ or σ_{max},[8,13] which are related according to Ref. 14:

$$K = \lim_{\rho \to 0} 1/2\ \sigma_{max}(\pi\rho)^{1/2} \tag{1}$$

where K is the stress-intensity factor, and σ_{max} is the maximum stress at the root of the notch. This relation has been shown to be highly accurate for the small value of ρ selected.[15]

Once cracks were initiated, these same specimens were further cycled in ambient air at a frequency of 40 Hz to determine resistance to fatigue-crack propagation over a broad spectrum of stress-intensity range ΔK, where[12]

$$K = \frac{P}{B\sqrt{W}} \frac{(2+\alpha)}{(1-\alpha)^{3/2}} (0.886 + 4.64\alpha - 13.32\alpha^2 + 14.72\alpha^3 - 5.6\alpha^4) \tag{2}$$

In this expression, P is the load and α is the normalized crack length a/W. A precision measurement technique[6] was employed to determine fatigue-crack growth rates da/dN in accordance with ASTM-E647.[12] Crack length a was determined as a function of elapsed cycles N from measurements of crack-mouth-opening-displacement (CMOD), using the calibration equations[16]

$$a/W = 1.0010 - 4.6695U + 18.460U^2 - 236.82U^3 + 1214.9U^4 - 2143.6U^5 \tag{3}$$

where

$$U = \frac{1}{[EB\ (\text{CMOD})/P]^{1/2} + 1} \tag{4}$$

and E is Young's modulus.

Table 1 Alloy chemistry

V	Fe	Al	O	H	C	N	Ti
9.7	1.8	3.2	0.087	0.0050	0.03	0.01	(bal.)

Table 2 Ti-10V-2Fe-3Al heat treatments

Nominal UTS (ksi)	Nominal UTS (Mpa)	% final α/β work	Solution treatment	Aging treatment
190	1310	2	1385°F(752°C)/2hr/W.Q	920°F(493°C)/8hr
190	1310	55	1385°F(752°C)/2hr/W.Q	920°F(493°C)/8hr
150	1034	2	1385°F(752°C)/2hr/W.Q	1025°F(552°C)/8hr
150	1034	55	1385°F(752°C)/2hr/W.Q	1025°F(552°C)/8hr

Table 3 Mechanical properties of Ti-10V-2Fe-3A1

Nominal UTS (ksi)	Nominal UTS (MPa)	% final α/β work	0.2% offset yield strength (ksi)	0.2% offset yield strength (MPa)	Ultimate tensile strength (ksi)	Ultimate tensile strength (MPa)	% elong.	% Red. Area	Plane strain fracture toughness, K_{Ic} (ksi$\sqrt{\text{in.}}$)	Plane strain fracture toughness, K_{Ic} (MPa$\sqrt{\text{m}}$)
190	1310	2	166.6	1149	186.8	1288	3.0	3.3	42.6	46.8
190	1310	55	172.6	1190	185.4	1278	7.0	12.8	33.7	37.0
150	1034	2	145.4	1002	154.8	1067	9.0	24.3	78.4	86.1
150	1034	55	143.6	990	146.4	1009	15.0	50.7	61.0	67.0

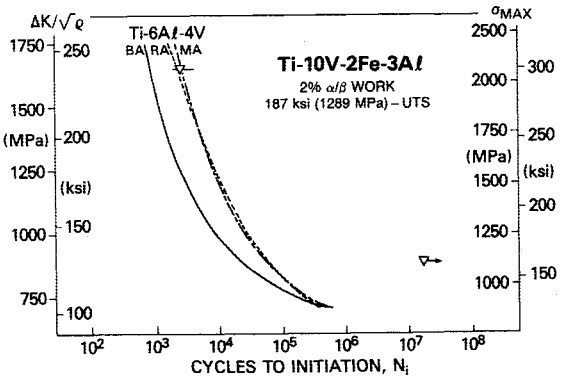

Fig. 2 Notched fatigue-crack initiation in Ti-10V-2Fe-3A1 at 1289 MPa (187 ksi) (UTS) with high aspect ratio (2% α/β work).

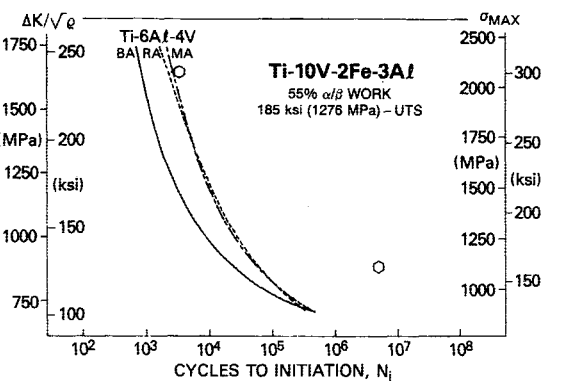

Fig. 3 Notched fatigue-crack initiation in Ti-10V-2Fe-3A1 at 1276 MPa (185 ksi) (UTS) with low aspect ratio (55% α/β work).

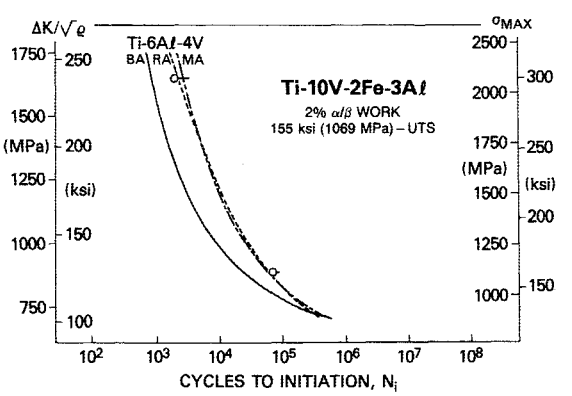

Fig. 4 Notched fatigue-crack initiation in Ti-10V-2Fe-3A1 at 1069 MPa (155 ksi) (UTS) with high aspect ratio (2% α/β work).

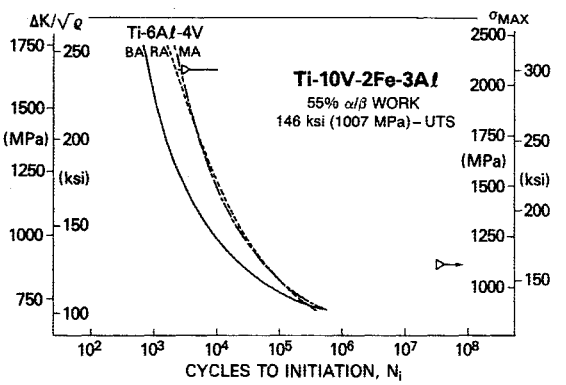

Fig. 5 Notched fatigue-crack initiation in Ti-10V-2Fe-3A1 at 1007 MPa (146 ksi) (UTS) with low aspect ratio (55% α/β work).

Results

Fatigue-crack initiation data are displayed for the four pancake-forged conditions of the Ti-10V-2Fe-3A1 alloy in Figs. 2–5, where cycles to initiation N_i are plotted vs the cyclic stress amplitude $\Delta K/\sqrt{\rho}$ on the left-hand ordinate and the related value of σ_{max} on the right-hand ordinate. Individual entries of data consist of a point (symbol) with line stubs extending to each side. {The symbol documents the first observation of a crack [typically ~ 0.030 in. (0.76 mm) in length], whereas the linear extrema represent 1) the last inspection point with no crack observed, and 2) the point at which the crack extends across the notch root to the full thickness.} In each figure, data are shown for the two levels of σ_{max} ($\Delta K/\sqrt{\rho}$) examined, and compared to data trend lines for Ti-6A1-4V as previously published[9] for three different microstructural morphologies, viz., those associated with the mill anneal (MA), recrystallization anneal (RA), and beta anneal (BA). The lower of the σ_{max} levels, 161 ksi (1110 MPa) or $\Delta K/\sqrt{\rho}$ = 128.4 ksi (885 MPa), corresponds approximately to that for which notched fatigue life of high strength Ti-10V-2Fe-3A1 was originally reported to cross over that for Ti-6A1-4V to inferior resistance in the low-cycle region.[1] (In that work, data were reported for center-hole-tension specimens of theoretical elastic stress concentration factor $k_t = 2.93$, with an approximate crossover level at nominal applied stress $S = 55$ ksi (379 MPa). Thus, since $\sigma_{max} = k_t S$ = 161 ksi (1110 MPa), this level has special significance. (Both nominal S and notch-intensified σ_{max} stress levels relate to maximum cyclic load.)

At this lower level of σ_{max}, the data in Figs. 2 and 3 show that the fatigue-crack initiation resistance of Ti-10V-2Fe-3A1 alloy at superhigh strength level [190 ksi (1310 MPa) UTS], for either high or low aspect ratio primary alpha-phase morphology, is vastly superior to that for Ti-6A1-4V. Even at the much higher amplitude $\Delta K/\sqrt{\rho}$ = 239.6 ksi (1652 MPa), the superhigh strength conditions of Ti-10V-2Fe-3A1 still exhibit resistance to fatigue-crack initiation that is similar to the best of the Ti-6A1-4V conditions.

On the other hand, as shown in Fig. 4 for the case of the higher aspect ratio alpha phase, a reduction in strength level of

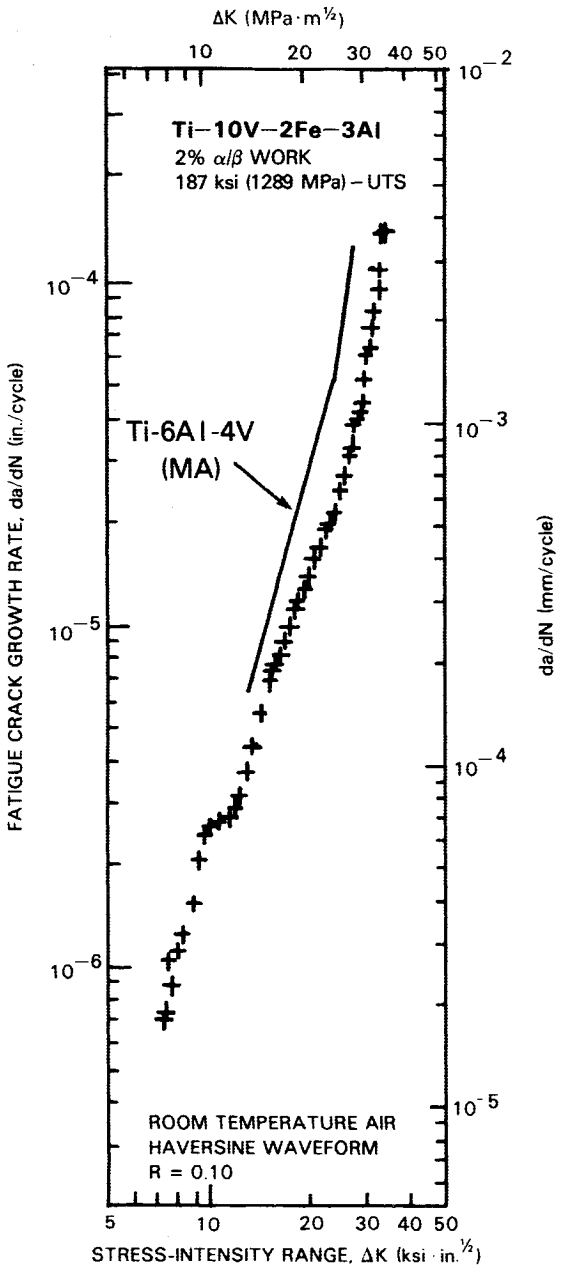

Fig. 6 Fatigue-crack growth rates in Ti-10V-2Fe-3Al at 1289 MPa (187 ksi) (UTS) with high aspect ratio (2% α/β work).

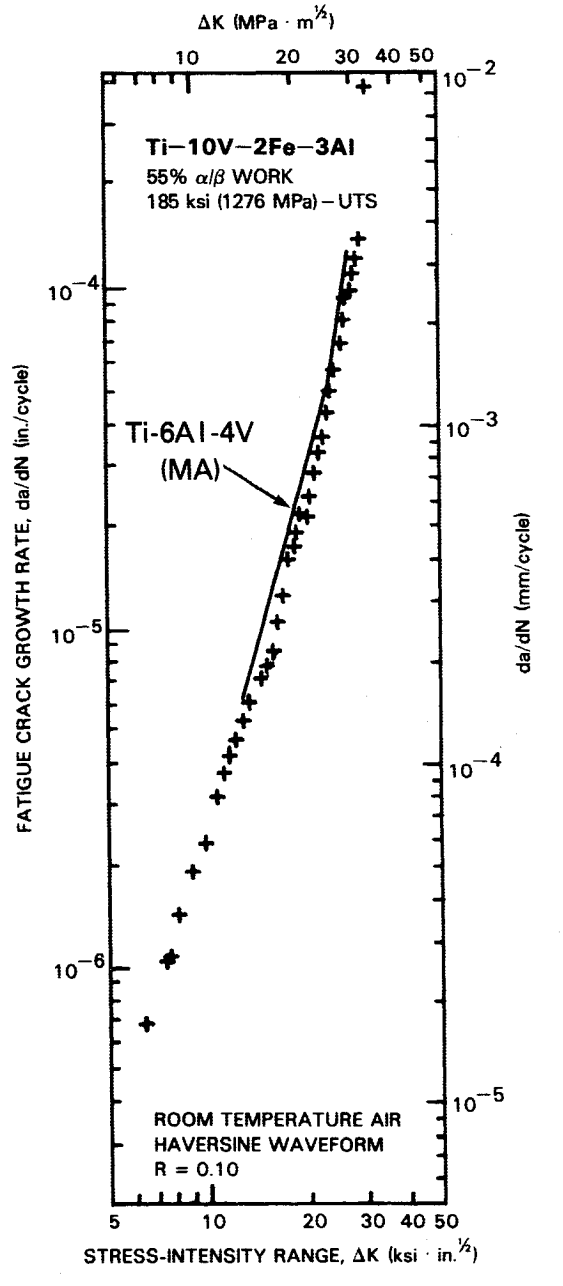

Fig. 7 Fatigue-crack growth rates in Ti-10V-2Fe-3Al at 1276 MPa (185 ksi) (UTS) with low aspect ratio (55% α/β work).

Ti-10V-2Fe-3Al to the vicinity of 150 ksi (1034 MPa) UTS can result in a significant reduction in fatigue-crack initiation resistance to levels associated with the Ti-6Al-4V microstructures, which are of similar strength level. The lower aspect ratio Ti-10V-2Fe-3Al at the 150 ksi (1034 MPa) UTS does not seem to exhibit such a reduction, however, as indicated in Fig. 5.

The counterpart fatigue-crack propagation resistance for the Ti-10V-2Fe-3Al pancake forgings is displayed in Figs. 6–9 where comparison can be made to a common data trend line for Ti-6Al-4V (MA condition). Fatigue-crack growth rates da/dN for all of the forgings are quite similar over the lower portion of the ΔK spectrum. However, in the upper portion, onsets to accelerated region III growth-rate behavior occur as affected by the fracture toughness. Thus, by virtue of extended region II growth-rate behavior, the fatigue-crack propagation resistance of the lower strength [150 ksi (1034 MPa) UTS] Ti-10V-2Fe-3Al conditions is significantly better than for the superhigh strength [190 ksi (1310 MPa) UTS] conditions. This can be seen most readily via comparison with the common data trend line for Ti-6Al-4V (MA). Note, too, that fatigue-crack propagation rates for the superhigh strength Ti-10V-2Fe-3Al conditions are quite similar to those for Ti-6Al-4V (MA).

Actual da/dN data for the various Ti-6Al-4V conditions mentioned above are shown in Fig. 10 together with the respective microstructures.

Discussion and Analysis

The foregoing initiation and propagation data permit the synthesis of notched fatigue life so that the desired comparative evaluation can be made. This has been done for the same specimen geometry and cyclic loading conditions for which notched fatigue life data for superhigh-strength Ti-10V-2Fe-3Al alloy [190 ksi (1310 MPa) UTS] were reported in prior work[1] to cross over to inferior resistance compared to Ti-6Al-4V. As already noted in the preceding section, this cyclic stress

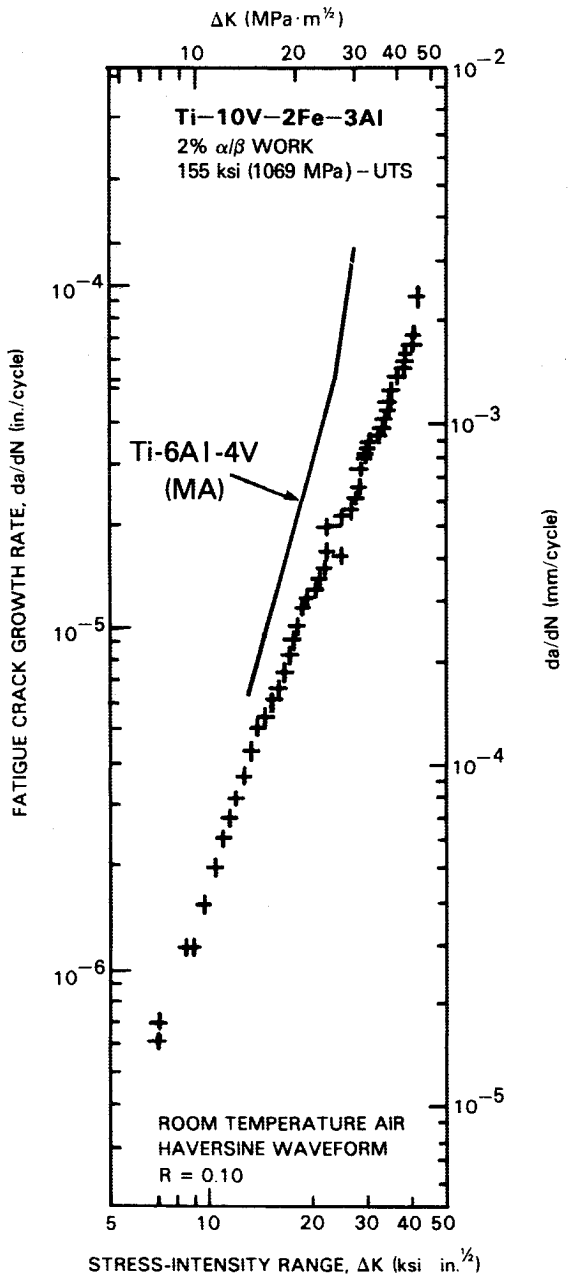

Fig. 8 Fatigue-crack growth rates in Ti-10V-2Fe-3Al at 1069 MPa (155 ksi) (UTS) with low aspect ratio (2% α/β work).

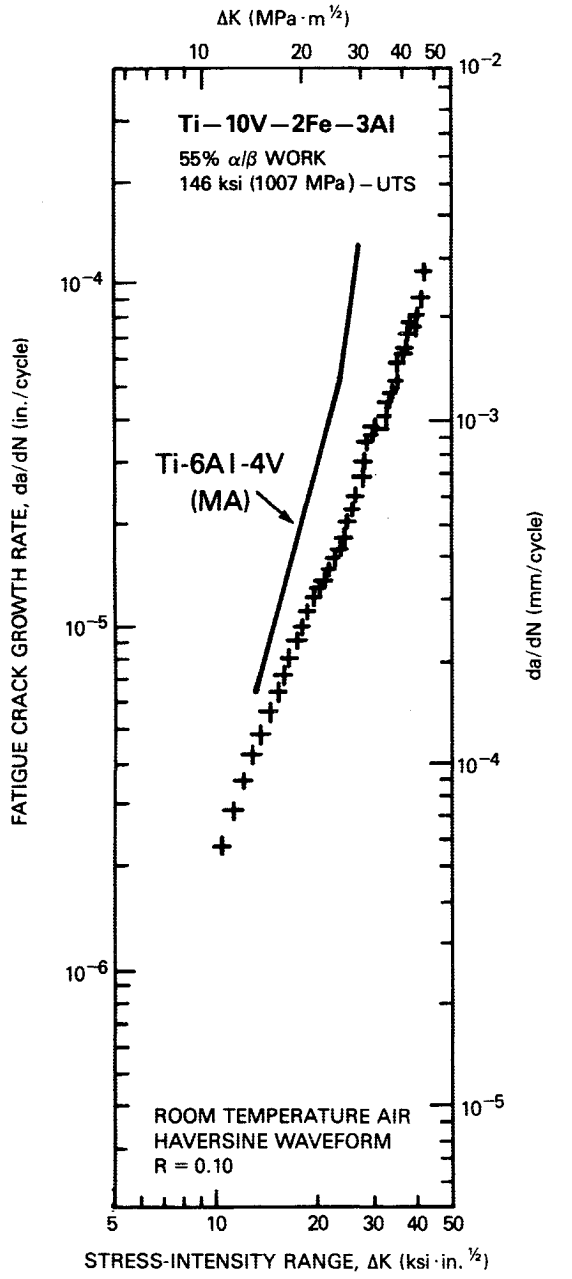

Fig. 9 Fatigue-crack growth rates in Ti-10V-2Fe-3Al at 1007 MPa (146 ksi) (UTS) with low aspect ratio (55% α/β work).

amplitude corresponds to the lower level $\sigma_{max} = 161$ ksi (1110 MPa), for which data were determined as displayed in Figs. 2-5. These data thus constitute the crack initiation components N_i of notched fatigue life, and are so displayed in Table 4.

To determine the counterpart crack-propagation components N_p of notched fatigue life, cycles of propagation life must be integrated from the point of crack initiation to that of either fracture instability or net section yield, whichever is less. This has been done, of course, for the same maximum stress level at the root of the notch (hole) $\sigma_{max} = 161$ ksi (1110 MPa), which is equivalent to a nominal applied stress level $S = 55$ ksi (379 MPa) in the center-hole-tension specimen geometry ($k_t = 2.93$). For this type of specimen geometry, illustrated schematically in Fig. 11, the stress-intensity factor is given by Ref. 12:

$$K = (P/BW)\sqrt{\pi a}\sqrt{\sec(\pi a/W)} \tag{5}$$

Actual dimensions used were $W = 1.000$ in. (25.4 mm), $B = 0.10$ in. (2.54 mm), and hole diameter $2c = 0.1875$ in. (4.76 mm). By fitting a power law to the da/dN data in Figs. 6-10, piecewise as appropriate, with the form

$$\frac{da}{dN} = A(\Delta K)^m \tag{6}$$

then total cycles of crack propagation can be obtained from the integration (also piecewise, as appropriate):

$$N_p = \int_{a_i}^{a_f} \frac{a^{-m/2}}{A(F\Delta S\sqrt{\pi})^m}\,da \tag{7a}$$

or

$$N_p = \frac{2}{(m-2)A(F\Delta S\sqrt{\pi})^m}\left[\frac{1}{a_i^{(m-2)/2}} - \frac{1}{a_f^{(m-2)/2}}\right] \tag{7b}$$

Table 4 Comparative evaluation of notched fatigue life and its components for Ti-10V-2Fe-A1 and Ti-6A1-4V

Material			N_i (cycles to crack initiation)	N_p (cycles of crack propagation)	Notched fatigue life $N_i + N_p$ (cycles)	Fracture toughness, K_{Ic} (ksi$\sqrt{\text{in.}}$)	(MPa$\sqrt{\text{m}}$)
Ti-10V-2Fe-3A1							
UTS (ksi)	UTS (MPa)	α/β work					
187	1289	2%	$>1.8 \times 10^7$	4.4×10^2	$>1.8 \times 10^7$	42.6	36.8
185	1276	55%	5.0×10^6	0.8×10^2	5.0×10^6	33.7	37.0
155	1069	2%	7.0×10^4	2.9×10^3	7.3×10^4	78.4	86.2
146	1007	55%	$>3.4 \times 10^7$	2.4×10^3	$>3.4 \times 10^7$	61.0	67.0
Ti-6A1-4V							
UTS (ksi)	UTS (MPa)						
150	1034	MA	5.4×10^4	1.5×10^2	5.4×10^4	38.2	42.0
146	1007	RA	6.0×10^4	1.5×10^3	6.2×10^4	69.2	76.0
139	958	BA	2.2×10^4	2.2×10^3	2.4×10^4	79.2	87.0

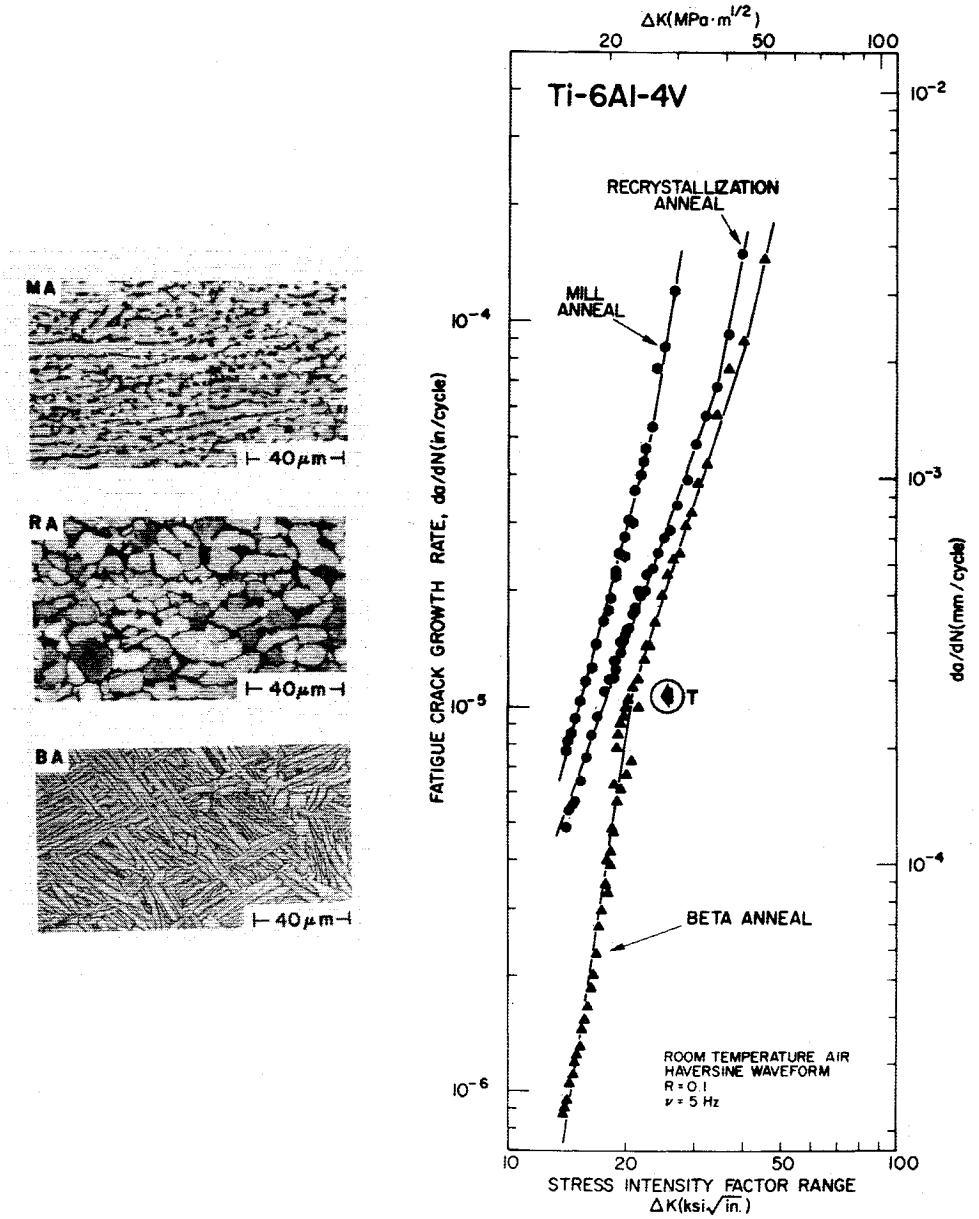

Fig. 10 Fatigue-crack growth rates and associated microstructures for Ti-6A1-4V.

where F is a geometric factor of approximately unity in the present case [viz., $\sqrt{\sec(\pi a/W)}$ in Eq. (5)], $S = P/(BW)$, and a_i and a_f are initial and final crack lengths, respectively. To determine a_i, Dowling's criterion[8] for demarcation between initiation and propagation phases is presumed, such that $a_i = c + \ell$ where

$$\ell = \frac{c}{(1.12\, k_t/F)^2 + 1} \tag{8}$$

In the present case, $\ell \approx 0.010$ in. (0.254 mm). [It should be noted that the crack size associated with the initiation data shown in this paper was not always precisely $\ell = 0.01$ in., as this was not experimentally feasible. However, such variation in the initiation size imparts only a very small, second-order uncertainty to the initiation life, particularly in the high-cycle region where observations and analysis have been made at $\sigma_{max} = 161$ ksi (1110 MPa). In this region, relatively very few cycles of propagation are involved in growing a crack from the point of first detection to that of full thickness size. Thus, the two points are barely discernible (if at all) from figures in this paper (cf., Fig. 4, e.g.) or Ref. 9 in the case of the Ti-6A1-4V. Moreover, when the crack is first observed to fully extend across the notch root to the point of full thickness, it has typically extended a discernible distance along (at least) one face of the specimen, to the point that an average crack length is not far from $\ell = 0.010$ in. (0.254 mm) as a first approximation.] It might be observed that the initial stress-intensity range for fatigue-crack propagation corresponding to these conditions is relatively high, [viz., $\Delta K_i \approx 29.8$ ksi $\sqrt{\text{in.}}$ (32.8 MPa $\sqrt{\text{m}}$)] when compared to some of the toughness levels. In those cases where a_f is associated with fracture instability, values are computed via Eq. (5) using the toughness.

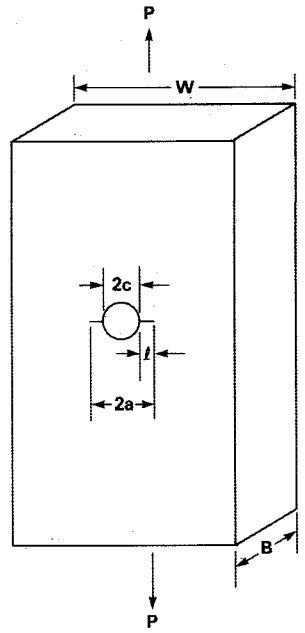

Fig. 11 Center-hole-tension specimen.

The resultant fatigue-crack propagation components N_p computed via Eqs. (7) are displayed in Table 4, as well as the total notched fatigue lives $N_i + N_p$, and the respective K_{Ic} levels for the four microstructures of Ti-10V-2Fe-3A1 and the three of Ti-6A1-4V. To facilitate comparison, these data are illustrated in the form of a semilogarithmic bar graph in Fig. 12. From this summary it is clear that 1) notched fatigue life is dominated in all cases by the fatigue-crack initiation component N_i; 2) crack-propagation life N_p appears to increase with K_{Ic} for both alloys—note, in fact, that N_p for high-strength Ti-10V-2Fe-3A1 [2% α/β work, 187 ksi (1289 MPa) UTS] actually exceeds that for Ti-6A1-4V (MA); and that most importantly 3) notched fatigue life for high-strength-level [190 ksi (1310 MPa) UTS] Ti-10V-2Fe-3A1 is substantially superior to that for the MA, RA, or BA conditions of Ti-6A1-4V. It is noted that a reduction in strength level of Ti-10V-2Fe-3A1 to the 150 ksi (1034 MPa) UTS [cf. 155 ksi (1069 MPA) UTS, 2% α/β work] can degrade the notched fatigue life to a level similar to that of the Ti-6A1-4V microstructures.

A few comments are in order concerning the inherently superior notched fatigue life behavior of Ti-10V-2Fe-3A1 at the superhigh strength level [190 ksi (1310 MPa) UTS], as uncovered in this study. This result should not be surprising, as it is consistent with the generally observed dependence of fatigue strength on the UTS[13] or the increased difficulty to initiate slip

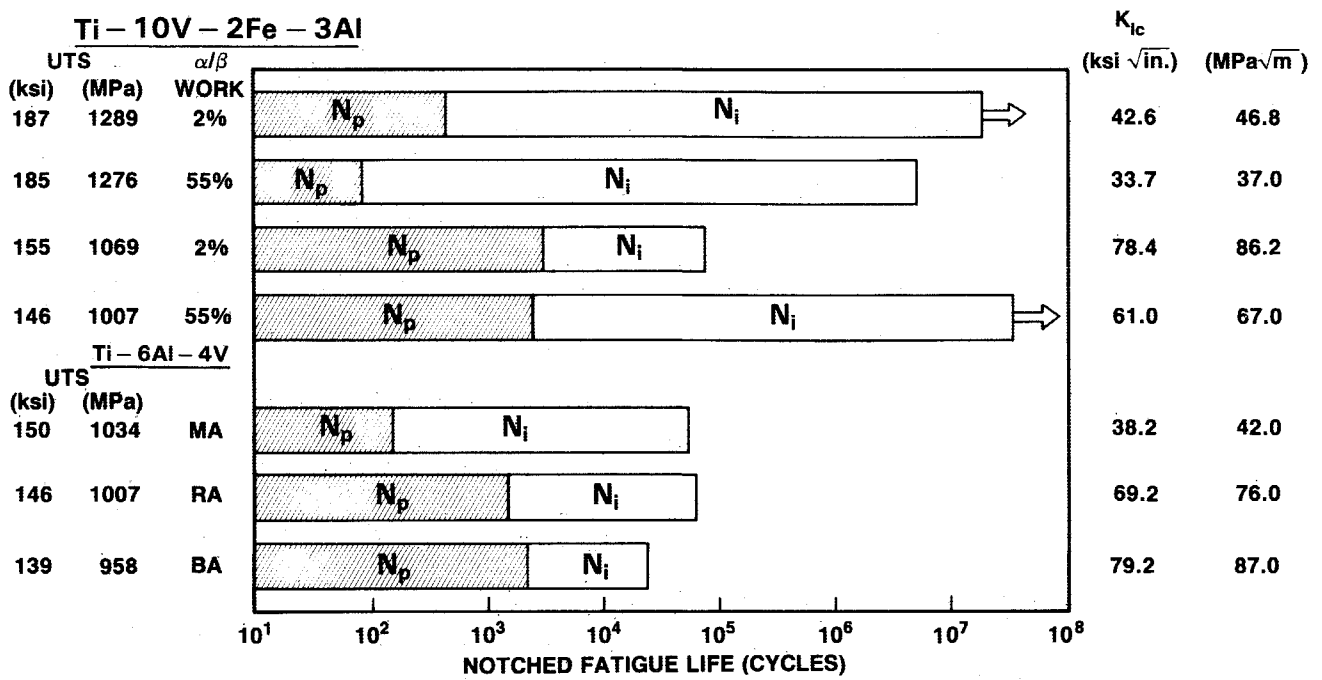

Fig. 12 Comparison of total notched fatigue life and its respective initiation N_i and propagation N_p components for Ti-10V-2Fe-3A1 and Ti-6A1-4V conditions of varied microstructure and strength level (cf. text for details of specimen and loading. These data are also summarized in Table 4).

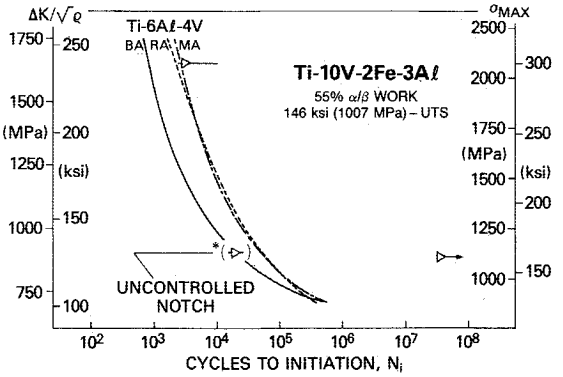

Fig. 13 Degradation in fatigue-crack initiation resistance of Ti-10V-2Fe-3Al associated with uncontrolled notch surface finish.

band cracks with increased strength level. How, then, are the seemingly contradictory findings from prior work[1,4] to be reconciled? Quite possibly, the earlier results reflect an uncontrolled notch (hole) surface finish in the test specimens, as NRL experience with Ti-6Al-4V and other alloys has indicated that failure to remove any tool marks with an orientation parallel to the axis of the notch root or hole (i.e., in the thickness direction) can prove highly detrimental to fatigue crack initiation resistance. To demonstrate this point, another specimen of Ti-10V-2Fe-3Al alloy was machined in the present study [146 ksi (1007 MPa) UTS and 55% alpha/beta work]—this time without a honed and inspected notch root. With this uncontrolled notch surface, notched fatigue-crack initiation resistance was reduced by over 99.9% from a level of $N_i > 34{,}000{,}000$ cycles to $N_i = 25{,}000$ cycles, as illustrated in Fig. 13.

Moreover, with the limited toughness associated with superhigh-strength material, a fabrication flaw such as the aforementioned tool marks could well serve as a crack-like defect leading to premature failure. For the cyclic stress amplitude associated with $S = 55$ ksi (379 MPa) as noted in the preceding analysis, the level of ΔK_i associated with a_i was 29.8 ksi $\sqrt{\text{in.}}$ (32.8 MPa $\sqrt{\text{m}}$) or $K_{max} = 33.1$ ksi $\sqrt{\text{in.}}$ (36.4 MPa $\sqrt{\text{m}}$) in the loading cycle—a level which is already uncomfortably close to the toughness levels K_{Ic} (cf. Table 3). In fact, the limited N_p levels computed for Ti-10V-2Fe-3Al at the 190 ksi (1310 MPa) UTS level in the present work were totally region III fatigue-crack propagation.[13] On the other hand, for the much lower strength Ti-6Al-4V (MA) alloy, the similarly limited toughness, $K_{Ic} = 38.2$ ksi $\sqrt{\text{in.}}$ (42.0 MPa $\sqrt{\text{m}}$), also confines N_p cycles exclusively to region III, with similar potential for unstable failure anticipated. For a higher toughness microstructure of Ti-6Al-4V, however, an improved N_p characteristic results, as illustrated herein for the RA and BA microstructures.

Conclusions

For the conditions examined in this study, which compare behavior of Ti-10V-2Fe-3Al for microstructures of different α-phase aspect ratio and strength level to that of Ti-6Al-4V for a variety of microstructures, the results indicate that:

1) The inherent notched fatigue life of superhigh-strength Ti-10V-2Fe-3Al (190 ksi or 1310 MPa ultimate tensile strength) is substantially superior to that of Ti-6Al-4V.

2) A reduction in the strength level of Ti-10V-2Fe-3Al to the vicinity of 150 ksi (1034 MPa) UTS can degrade the notched fatigue life to levels associated with the Ti-6Al-4V microstructures, which are of similar strength level.

3) In the case of each microstructure of Ti-10V-2Fe-3Al and Ti-6Al-4V, notched fatigue life is dominated by the crack-initiation component.

4) For both alloys, the fatigue-crack propagation component of notched fatigue life appears to increase with fracture toughness; in fact, it is found that the propagation component for superhigh-strength Ti-10V-2Fe-3Al can actually exceed that for Ti-6Al-4V.

Acknowledgments

The support of this work by the Naval Air Systems Command is gratefully acknowledged, as is the encouragement of J. F. Collins, W. Koegel, and L. E. Sloter. The experimental assistance of J. L. Berman, L. A. Cooley, and S. R. Jackson is also much appreciated.

References

[1]Boyer, R. R., "Design Properties of a High-Strength Titanium Alloy, Ti-10V-2Fe-3Al," *Journal of Metals,* Vol. 32, March 1980, pp. 61–65.

[2]Chen, C. C. and Boyer, R. R., "Practical Considerations for Manufacturing High-Strength Ti-10V-2Fe-3Al Alloy Forgings," *Journal of Metals,* Vol. 31, July 1979, pp. 33–39.

[3]Kuhlman, G. W. and Gurganus, T. B., "Optimizing Thermo-Mechanical Processing of Ti-10V-2Fe-3Al Forgings," *Metal Progress,* Vol. 118, No. 2, July 1980, pp. 30–35.

[4]Boyer, R. R. and Kuhlman, G. W., "Processing Properties Relationships of Ti-10V-2Fe-3Al," *Metallurgical Transactions A,* Vol. 18A, The Minerals, Metals, and Materials Society, Warrendale, PA, Dec. 1987, pp. 2095–2103.

[5]Boyer, R. R., Eylon, D., and Froes, F. H., "Comparative Evaluation of Ti-10V-2Fe-3Al Cast, P/M and Wrought Product Forms," *Titanium Science and Technology,* Vol. 2, edited by G. Lutjering, U. Zwicker, and W. Bunk, Deutsche Gesellschaft fur Metallkunde e.V., Oberursel, West Germany, 1985, pp. 1037–1313.

[6]Yoder, G. R., Cooley, L. A., and Crooker, T. W., "Procedures for Precision Measurement of Fatigue Crack Growth Rate Using Crack-Opening Displacement Techniques," *Fatigue Crack Growth Measurement and Data Analysis,* edited by S. J. Hudak, Jr., and R. J. Bucci, American Society for Testing and Materials, Philadelphia, PA, ASTM STP 738, 1981, pp. 85–102.

[7]Yoder, G. R., Cooley, L. A., and Crooker, T. W., "Observations on a Fracture Mechanics Approach to Fatigue Crack Initiation in Ti-6Al-4V," *Fracture Mechanics: Sixteenth Symposium,* edited by M. F. Kanninen and A. T. Hopper, American Society for Testing and Materials, Philadelphia, PA, ASTM STP 868, 1985, pp. 392–405.

[8]Dowling, N. E., "Fatigue at Notches and the Local Strain and Fracture Mechanics Approaches," *Fracture Mechanics,* edited by C. W. Smith, American Society for Testing and Materials, Philadelphia, PA, ASTM STP 667, 1979, pp. 247–273.

[9]Yoder, G. R., Cooley, L. A., and Crooker, T. W., "A Comparison of Microstructural Effects and Fatigue-Crack Initiation and Propagation in Ti-6Al-4V," *Proceedings of the 23rd Structures, Structural Dynamics, and Materials Conference,* CP 823, Pt. 1, AIAA, New York, 1982, pp. 132–136.

[10]Yoder, G. R., Cooley, L. A., and Crooker, T. W., "Enhancement of Fatigue Crack Growth and Fracture Resistance in Ti-6Al-4V and Ti-6Al-6V-2Sn Through Microstructural Modification," *Journal of Engineering Materials and Technology, Transactions of ASME,* Vol. 99, Ser. H, Oct. 1977, pp. 313–318.

[11]Hirth, J. P. and Froes, F. H., "Interrelations Between Fracture Toughness and Other Mechanical Properties in Titanium Alloys," *Metallurgical Transactions A,* Vol. 8A, No. 7, The Minerals, Metals, and Materials Society, Warrendale, PA, 1977, pp. 1165–1176.

[12]"Standard Test Method for Constant-Load Amplitude Fatigue Crack Growth Rates Above 10^{-8} m/Cycle," *Annual Book of ASTM Standards,* Vol. 03.01, Sec. 3, American Society for Testing and Materials, Philadelphia, PA, ASTM E647-86, 1986, pp. 714–736.

[13]Hertzberg, R. W., *Deformation and Fracture Mechanics of Engineering Materials,* 2nd ed., Wiley, New York, 1983, p. 697.

[14]Irwin, G. R., "Fracture Mechanics," *Structural Mechanics: Proceedings of the First Symposium on Naval Structural Mechanics,* edited by J. N. Goodier and N. J. Hoff, Pergamon, New York, 1960, pp. 557–594.

[15]Wilson, W. K., "Elastic-Plastic Analysis of Blunt Notched CT Specimens and Applications," *Journal of Pressure Vessel Technology, Transactions of ASME,* Vol. 96, Ser. J, No. 4, American Society of Mechanical Engineers, New York, Nov. 1974, pp. 293–298.

[16]Saxena, A. and Hudak, S. J., Jr., "Review and Extension of Compliance Information for Common Crack Growth Specimens," *International Journal of Fracture,* Vol. 14, Oct. 1978, pp. 453–468.